Experimental and numerical studies of smoke dynamics in a compartment fire

B. Betting, E. Varea, Carole Gobin, G. Godard, B. Lecordier, Béatrice Patte-Rouland

Experimental and numerical studies of smoke dynamics in a compartment fire

B. Betting, E. Varea, C. Gobin, G. Godard, B. Lecordier, B. Patte-Rouland

Normandie Univ, INSA Rouen, UNIROUEN, CNRS, CORIA, 76000 Rouen, France

Abstract

Fires in confined spaces are of major concern in fire safety engineering. Indeed, fires with ensuing fatalities, generally occur in apartment or room fires. The decision and response time of rescue teams mainly results from empirical understanding. However, since compartment fires are multi-physical and multi-scale problems, a clear fundamental approach is needed. One of the main issues concerns the transition from localized to generalized fire. The most important vector leading to generalized fires is smoke. Indeed, smoke temperature is very high and many species i.e. burned and unburned gases are already mix or might mix. In this study, an experimental facility composed of a maritime container is set-up. It allows enclosure fires up to 1 MW of power. This power is representative of moderate room fires. The global behavior of the smoke is investigated through the analysis of mean experimental temperature fields, smoke dynamics by large scale PIV as well as numerical simulations. For numerical simulations, the Fire Dynamics Simulator (FDS) software is used. The experimental measurements are used to evaluate the validity of FDS in under-ventilated conditions. It is observed that FDS code is able to reproduce both temperature and velocity data of enclosure fires with accuracy depending on the power to volume ratio. A criterion capable to discriminate the ventilation status of confined fire is observed and discussed.

Keywords: Compartments fire, PIV large scale, enclosure fire, FDS, smoke dynamics,

1. Introduction

Every year in France, compartment fires are responsible for more than 88,000 interventions involving more than 15,000 people, including several hundred deaths and serious injuries ([1], [2], ANR Firediag). Nowadays, the decision-making process of emergency services during fire interventions is mainly based on a rapid disaster analysis. This analysis comes from the experience gained over the years. However, this type of analysis does not permit a complete understanding of the disaster since it is mainly based on empirical knowledge. The evolution of a fire, the appearance of a secondary focus or of thermal phenomena, i.e. back-draft [3, 4] or flash-over [5, 6, 7], are difficult to predict with accuracy.

In order to optimize and secure the intervention of rescue services safety engineering, including knowledge of fire dynamics and fire-related hazards is crucial [8]. More precisely, one of the main critical aspects that remains to be determined is the smoke dynamics at openings where fresh air and hot fumes mix. Indeed, this particular phenomenon, typical of under-ventilated fires, may be encountered in many enclosures fires. This phenomenon is called pulsing fire and has been extensively studied by Merci [9], Bengtsson [10] and Pretrel [11]. Pulsating fires occur in oxygen-limited conditions. These conditions may be related to natural (opening) or mechanical ventilation (nuclear power plants, High-rise buildings) [9].

Study of smoke dynamics is made possible using different devices or techniques. These include, among others Pitot probes and bidirectional probes or McCaffrey probes [12]. However, these probes are intrusive and potentially impacting the smoke dynamics. Moreover only one point data is evaluated. For this reason, laser techniques can be used. The smoke velocities can be studied using the PIV technique [13, 14, 15]. This technique has already been used in the study of fires [16, 17, 18] for well-ventilated and under-ventilated conditions. A natural extension of this technique is to use the PIV to highlight exchanges between hot exhaust fumes and fresh incoming air. These large-scale measurements highlight areas of interest for a better understanding of fires.

In order to gain further insights into smoke dynamics in a confined environment, we propose a dual approach based on experimental and numerical data. The scalar quantity (temperature) and the vector quantity (velocity)

are evaluated and compared considering both experimental and numerical data. The objectives of the paper are threefold :

- To design an experimental set-up to ensure PIV measurements inside the fire volume.
- To observe the specific behavior of confined fires for ventilated or under-ventilated conditions for both temperature and velocity data. The capability of FDS code to reproduce confined fires with accuracy is discussed.
- To obtain more information about the transition from ventilated to under ventilated fire conditions. This information will be use to design a helpful decision-making tool for fire officers.

2. Experimental set-up

To investigate the smoke dynamic characteristics of enclosure fires, an experimental test bench is set-up. The thermal phenomena studied using the test bench are likely to be encountered by firefighters during their missions. This cell is composed of two maritime containers mounted perpendicularly. One is the measure cell and the other is the test cell. In this configuration, only one $1 m^2$ outlet ($0.8 m^2$ of clear aperture due to insulation) in the opposite direction to the burner), is open, Fig. 1.

The standard size of a maritime container is $6\,m \times 2.59\,m \times 2.45\,m$. These structures have emerged as training tools in rescue services. Moreover, the volume of these containers is close to that of a room of a standard flat, which is approximately $35\,m^3$ [4].

The fuel source consisted of 36 propane burners with a surface area of $1\,m^2$, Fig 2. This configuration enables the fire to reach 1 MW with temperatures up to 1000 °C. Propane fuel is chosen because it has the advantage of being correctly controlled and enhances the reproducibility of the experiments. Due to the high temperatures reached during experiments, insulation is an important component in the test bench design (Fig. 3). Insulation is provided using :

- 40 cm of cellular concrete blocks (floor) ;
- 10 cm of rock wool (0.034 W/m.K) and 5 cm mineral wool (0.034 W/m.K) (roof) ;

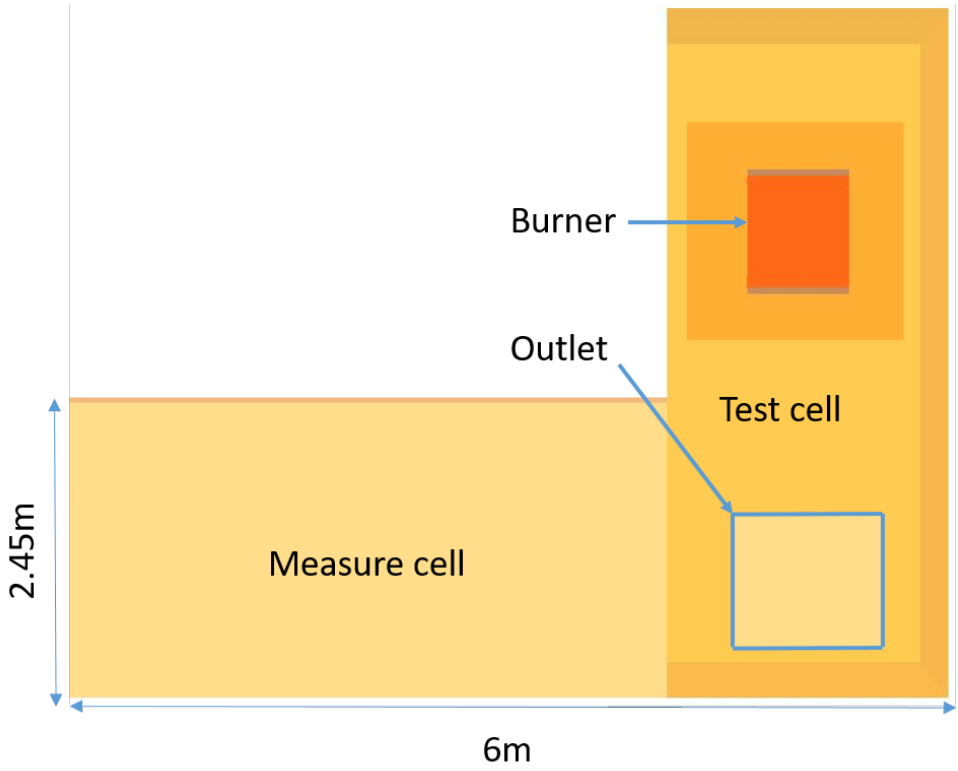

FIGURE 1: Experimental set-up configuration, top view.

— 10 cm of mineral wool (0.034 W/m.K) and 3cm of vermiculite plates (0.21 W/m.K).

A $1\,m^2$ access enables both the visualization and setup of advanced laser diagnostics such as Particle Image Velocimetry (PIV) [18].

For temperature measurements, 20 type-K thermocouples (diameter of 1.5 mm) are used. Two racks of 10 thermocouples are mounted vertically and horizontally along the center line of the chamber. Position is adjusted to be below the outlet which is opposite side of the burner, Fig 4.

Particle Image Velocimetry (PIV) configuration is represented in Fig 5.

Large scale PIV is a complex task because it is a compromise between spatial resolution and field of view. To overcome this issue, a special configuration is set-up. Instantaneous, two-dimensional velocity measurements relied on Particle Image Velocimetry (PIV) in which alumina particles are used (50

FIGURE 2: Burner view.

FIGURE 3: Inside view of the test cell.

μm diameter). These particles are injected through an in-house air supply corona which is positioned below the burner. Particles are injected in such a way that the fresh air injection dynamics are not modified. As low as 10 % of air to reach stoichiometric condition is used to feed the burner with particles seeded air. The optical arrangement is : Nd : Yag laser (Quantel QSmart, 2*400 mJ/pulse) 1, mirrors 2 and 3 and a -20mm cylindrical lens which pro-

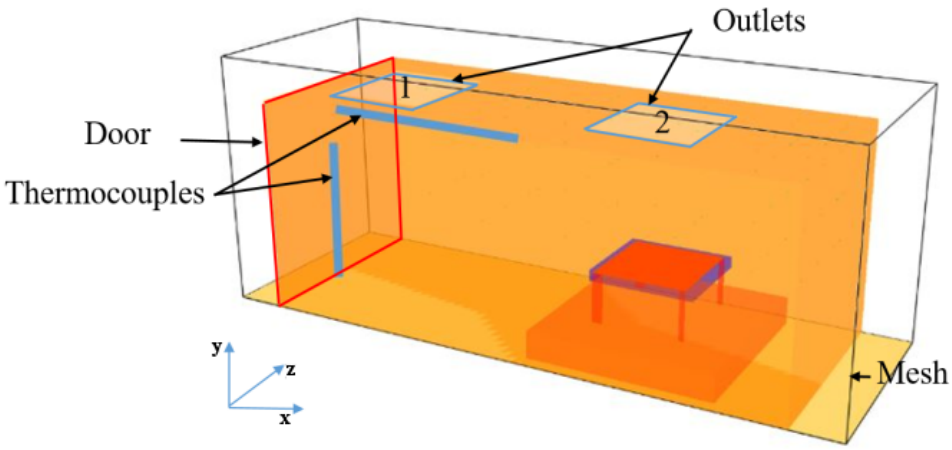

FIGURE 4: FDS view of the cell.

duce 0.5mm thick laser sheet 5 and 6. Mie scattering from the particles is collected on 4 CCD (Charge-Coupled Device) cameras 7,(JAIRM4200, 12 bits, 2048*2048 pix^2) mounted with 50mm f/1.2 Zeiss lens. A 532 nm interferential filter reduces noise from ambient light sources. The optical arrangement yields a magnification of 5 pix/mm. Data are recorded using Dantec Dynamics software. Raw images are post-processed with an in-house PIV algorithm developed by Dr. B. Lecordier. A short description is given below. The four individual images are combined into a single image using a reference grid. Compensation is made for distortion and tilt. Preprocessing to reduced correlation on identified structures resulting from local soot generation or interfaces due to non-seeded fresh air coming from the opening. Then PIV processing is performed using a cross-correlation technique between pairs of successive images. The size of the PIV interrogation windows is 64 pix^2 with a 50 % overlap. The time interval between two consecutive images is in the range of 1 to 2.5 ms, depending on the powers and therefore flow velocity.

3. Numerical simulations

Simulations are performed using FDS code version 5 [19] which was developed by the National Institute of Standards and Technology (NIST). Due to its extensive validation [20, 21], FDS is commonly used in engineering studies

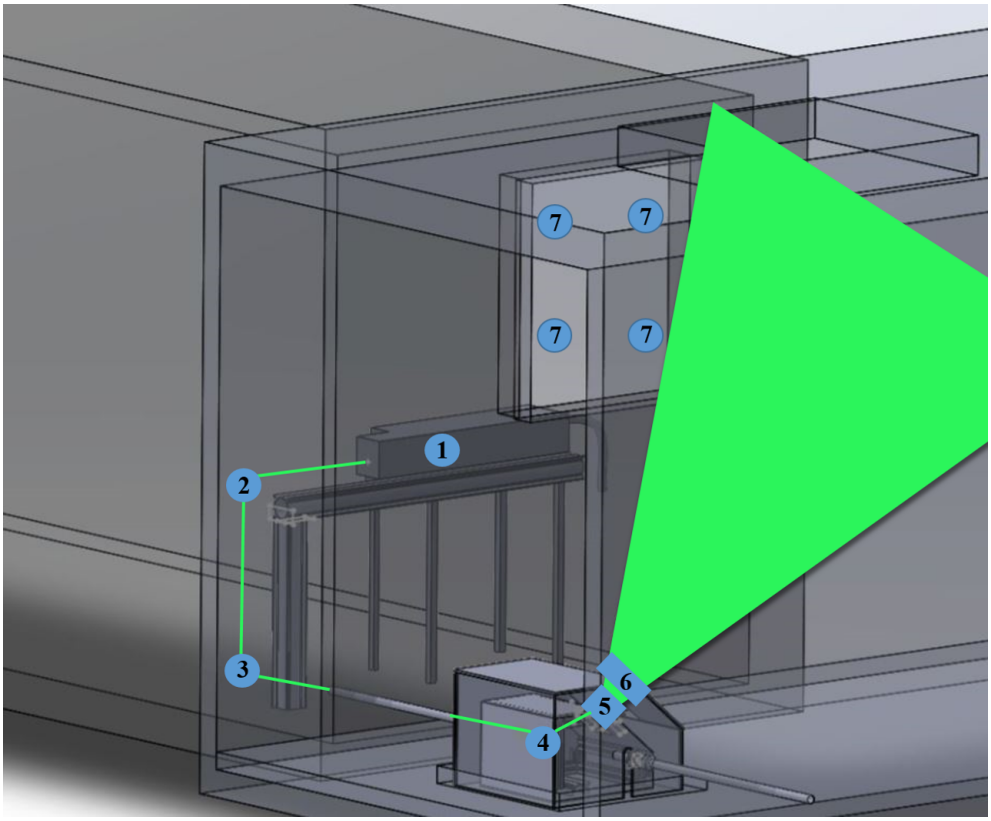

FIGURE 5: PIV set-up.

of fire safety.

The numerical domain is represented in Fig. 4.

A mesh sensitivity is shown in Fig 6. Temperature profiles from simulations are plotted against time ($600\,s$) with cell sizes of 2.5 cm, 5 cm, 10 cm and 20 cm. Results indicate no significant differences at long time scales. Note that with the smaller mesh, a slightly higher temperature is observed in the ramp-up phase.

Table 1 shows for grid resolutions of 2.5, 5, 10 and 20 cm together with the cell number and computation time.

From the experiments, spatial resolution for the PIV is approximately 2.5 cm. However, a computation time of 9 days for 2.5 cm mesh is not acceptable. Therefore, the 5 cm cell size is chosen to optimize computational time and

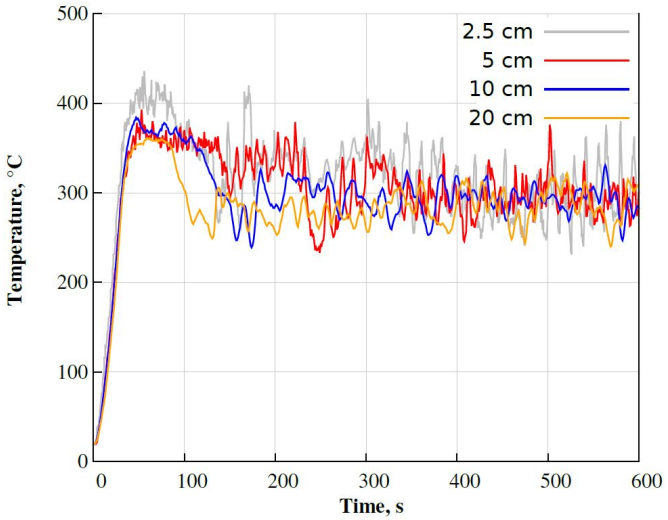

FIGURE 6: Grid resolution for 2.5, 5, 10 and 20 cm.

Grid resolution (cm)	Simulation time	Cell number
2.5 cm	9 days 7h43	2 924 544
5 cm	17h02	365 568
10 cm	1h34	45 696
20 cm	7min	5 712

TABLE 1: Summary of simulation times.

spacial resolution. The domain is discretized into more than 365000 cells. To ensure reliability between experimental and numerical results, the following points are verified.

The boundary conditions used in this work are :

— Total opening of the domain to simulate the outside ;
— Ramp fire very fast because the fuel is propane ;
— Consideration of insulation for heat losses.

To this end, we propose a test matrix which summarizes the test cases for both experimental and numerical data, Table 2.

	Experiments	Simulations
Temperature	200 kW, 500 kW and 800 kW, 1 point averaged temperature 10 thermocouples under the ceiling	2D fields + 1 point averaged temperature at 200 kW, 500 kW and 800 kW
Velocity maps	100 kW to 1000 kW	100 kW to 1000 kW
Vertical velocity	200 kW, 500 kW and 800 kW mean profiles	no comparison

TABLE 2: Summary of simulation.

4. Results

In this section, data from temperature profile and velocity fields are reported and discussed. Conditions are defined in the previous section (see Table 2) and are briefly given at the beginning.

4.1. Temperature data

4.1.1. Experimental and numerical profiles

Simulations are performed for three different heat release rates : 200 kW, 500 kW and 800 kW. The results of numerical and experimental temperature profiles plotted against time are compared in Fig. 7. The temperatures correspond to the evolution of the average values of the ten thermocouples below the ceiling.

In Fig. 7(a), 200 kW, it is observed that the temperature evolution against time for experimental and numerical results are very similar. The HRR increases are almost identical, as well as the temperature values. In addition, the steady-state is not reached. In Fig. 7(b), the temperature evolution against time is plotted for a HRR of 500 kW. Numerical and experimental

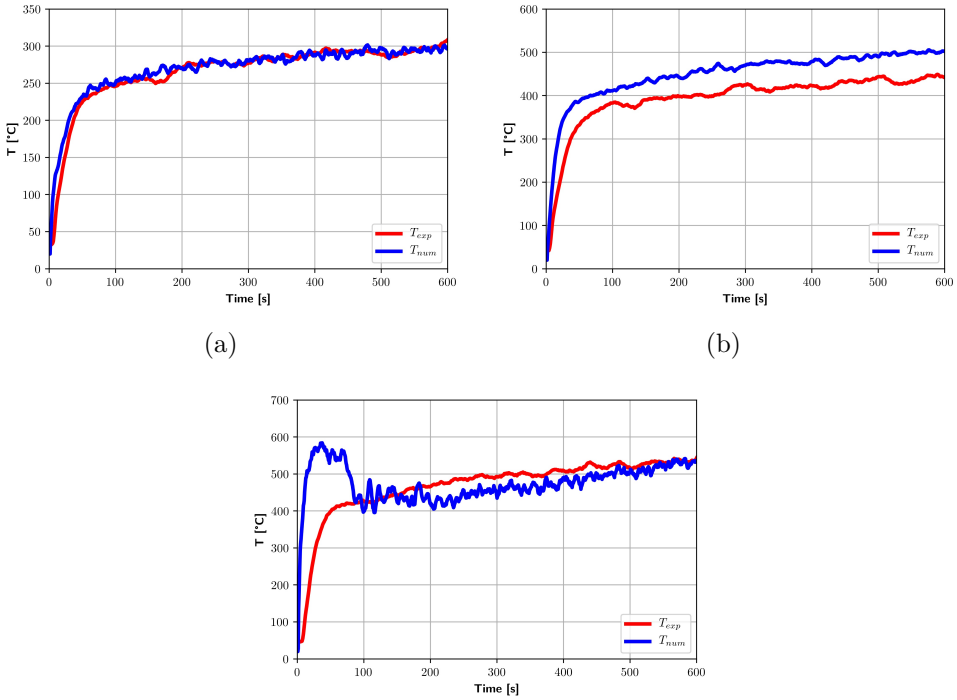

FIGURE 7: Temperature profiles at 200 kW (a), 500 kW (b) and 800 kW (c) ; Experimental : red line, Simulation : blue line.

results exhibit similar profiles. However, it is observed that a slight shift appears between the two temperature evolution. This is due to the beginning of under-ventilated conditions which are difficult to model in FDS. In Fig.7(c), 800 kW an significant discrepancy between the experimental and numerical results exists from the beginning. This difference is resolved after 100 seconds. This deviation of the numerical data from the experimental results might be due to FDS code which uses to overestimate the heat release rate in under-ventilated conditions. This was discussed in [22]. In order to verify this assumption, 2D temperature distributions are evaluated via simulations.

4.1.2. Numerical results of 2D fields

In this section, the development of the fire are studied for the complete configuration considering 2D fields. 200, 500 and 800kW cases are studied. The burner is located on the right side of the cell while the open outlet is on the left side. In Fig. 8, the instantaneous at t=300s (right) and the average (left) temperature fields are presented.

In Fig. 8(a) the instantaneous temperature field at 200 kW is reported. The smoke take place in the upper part of the domain. Re-circulation of fresh air is observed at the outlet. This fresh air transports oxygen to the fire. At this time, the volume is considered to be properly ventilated. This observation can be confirmed by the long time averaged field, see Fig. 8(b). On the averaged field, clear plume and stratification are observed. The re-circulation zones are also present.

The 2D fields for 500 kW configuration are given in Figs. 8(c) and 8(d). In this case, the fire dynamics are completely different. The temperature distribution is above 350°C. The initial fire focus is no longer localized at the burner. It is observed that the flame moved towards the outlet. During this simulation it is observed that the flame position is highly unstable (RMS not shown here). This phenomenon represents the alternation of fresh air intake and evacuation of hot gases.

The pressure in the enclosure decreases and allows fresh air to enter. This fresh air entrance restarts combustion which causes the pressure to increase and a release of hot gases. This phenomenon, characteristic of under ventilated fire, is repeated until there is no more fuel.

Figures 8(e) and 8(f) show the 800 kW configuration. The flames and hot gases are concentrated at the outlets and below the burner. These locations correspond with the presence of oxygen in the cell.

From the temperature profiles, it is observed that the quality of the simulations degrades with the increase in HRR. This might be due to the appearance of under-ventilated conditions which are difficult to model in FDS, [22]. This is supported by the 2D temperature distributions where under-ventilated behaviors are observed for higher HRR. Under ventilated conditions dominate

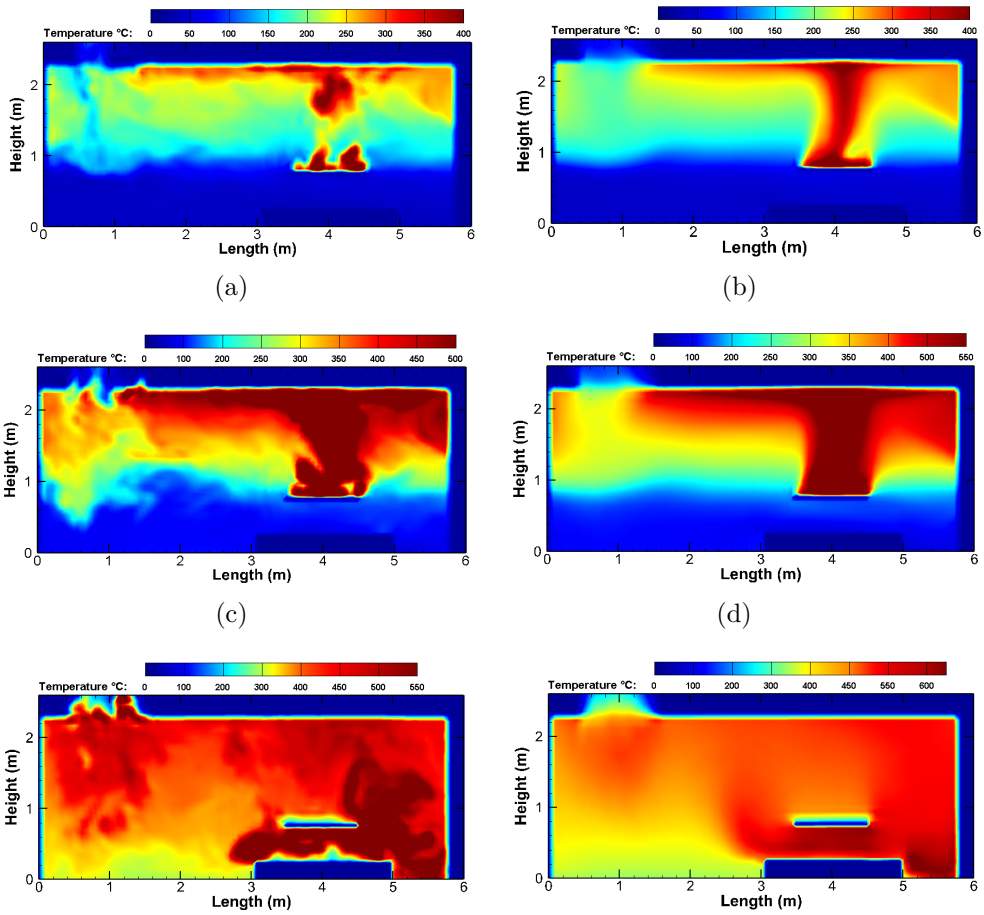

FIGURE 8: (300s)Instantaneous(t=300s), left, and average, right, temperature fields at 200 kW (a, b), 500 kW (c, d) and 800 kW (e,f).

this type of configuration and strongly influence fire dynamics including temperature and velocity. The limitations of FDS with regard to under-ventilated fires is know.

In order to evaluate if the flame is quenched with increased powers, the numerical Heat Release Rate (HRR) is reported for powers ranging from 200 to 800kW. In Figure 9(a) HRR at 200 kW is plotted. The HRR remains constant which is typical for well-ventilated conditions. At 500 kW, Fig. 9(b), venti-

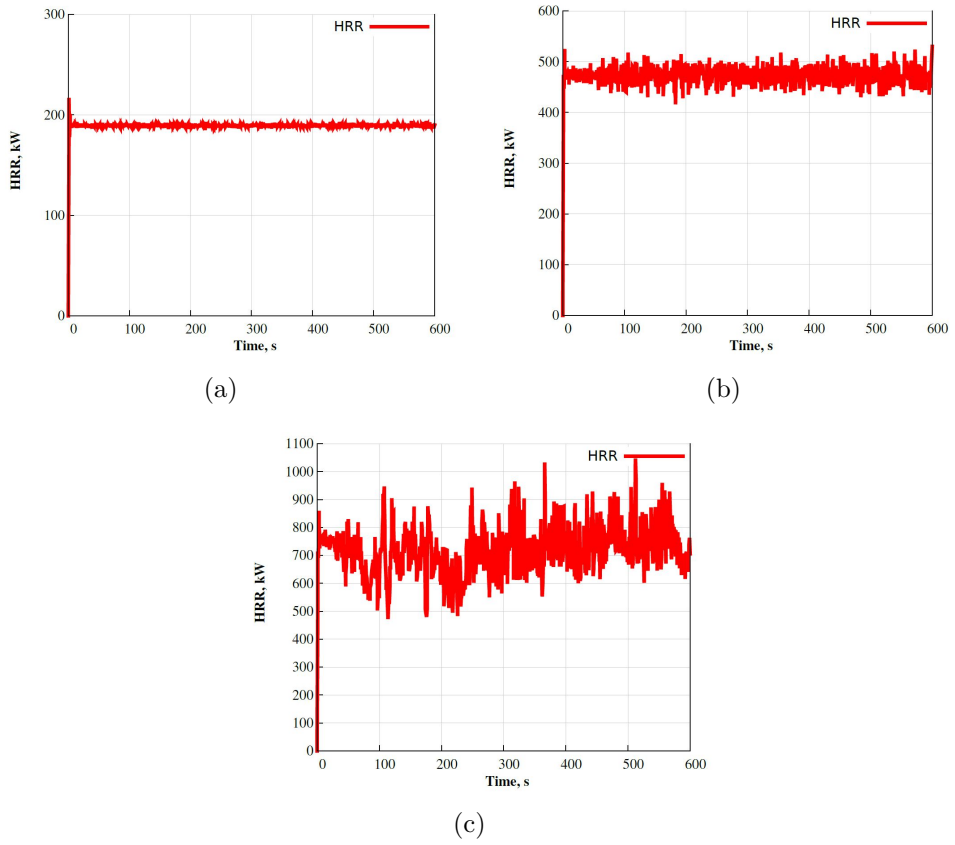

FIGURE 9: HRR evolution against time for 200 kW (a), 500 kW (b) and 800kW (c).

lation conditions become less favorable. The HRR is less stable. However, the value remains close to the specified value, making experimental and numerical temperature profiles fairly similar. Finally, for 800 kW, Fig. 9(c), the HRR exhibits large fluctuations. This is typical for under-ventilated conditions. The simulations are less accurate since FDS is less valid for these configurations due to both high HRR and under-ventilated conditions. This confirmation of under-ventilated conditions explains the differences observed in Fig 7(c).

4.2. Velocity fields

In this section, both experimental 2D fields from large scale PIV measurements and simulations are reported and discussed.

4.2.1. Experimental fields

This section present the results obtained from the PIV measurements. Smoke velocities are measured for HRR ranging from 100 kW to 1 MW. This makes it possible to study will-ventilated to severely under-ventilated cases.

Figure 10 shows the position of the experimental field of view. The blue frame represents the 1 m^2 measuring area. Figure 11 shows velocity fields for HRR ranging from 100 kW, Fig 11(a), 200 kW, Fig 11(b), 300 kW, Fig 11(c) and 400 kW, Fig 11(d). The horizontal velocity U along the x axis is reported. The black frame in Fig 11(a) represents the outlet position and is not reported for other.

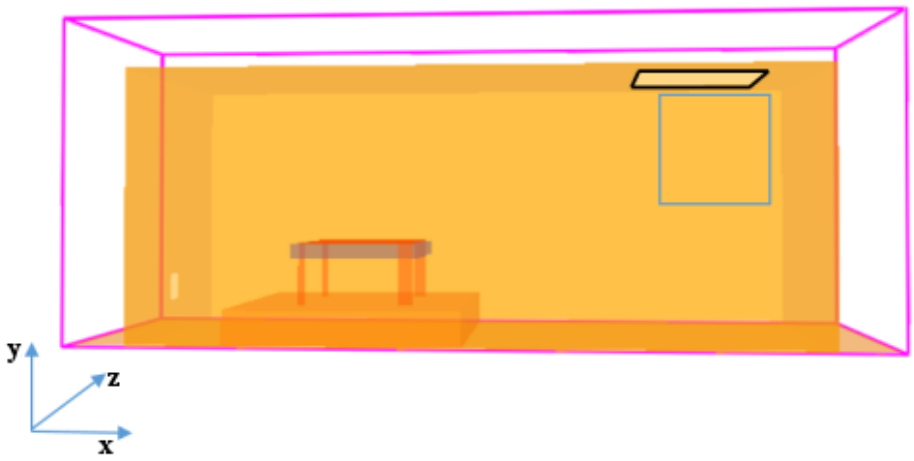

FIGURE 10: Position of the measuring area.

The hot gases coming from the burner in the upper part of the volume are observed to be evacuated by the outlet. Velocity vectors indicate recirculation of fresh air, necessary for feeding properly the fireplace.

The smoke layer is clearly visible in Fig 11(a) for 100 kW case. Its position is relatively high. The latter is represented by the orange / red colors in the

upper part of the image.

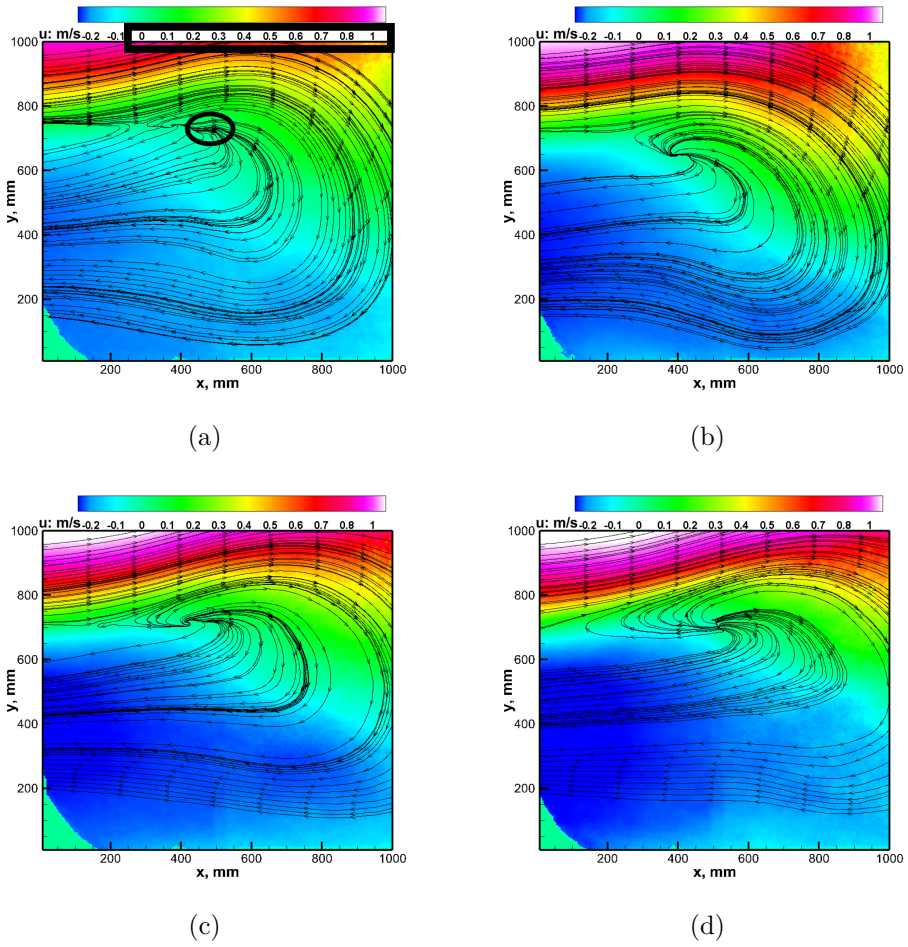

FIGURE 11: Average velocity fields at 100 kW (a), 200 kW (b), 300 kW (c), 400 kW (d).

The position of the stagnation plane, the main location of mixing, can be seen to be relatively insensitive to the power evolution..

To check this hypothesis, Figures 12 and 13 shows the velocity fields from 500 kW to 1000 kW.

For these powers, the smoke layer seems to drop slightly before it stabilizes. The smoke layer position seems almost identical in Figures 12 and 13. In

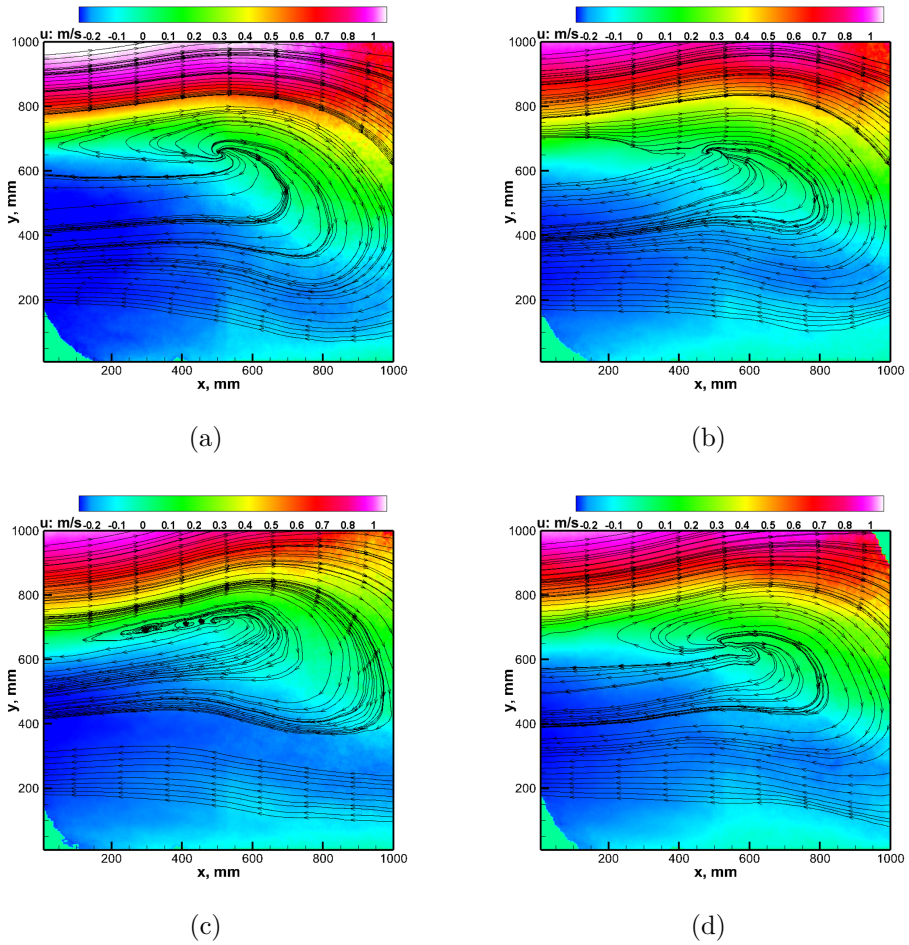

FIGURE 12: Average velocity fields at 500 kW (a), 600 kW (b), 700 kW (c), 800 kW (d).

addition, the mixing zone intensified, especially at 700 kW, 12(c). This is confirmed for HRR of 900 kW and 1 MW, Figs 13(a)) and 13(b), where the stagnation plane is stretched and became longer.

For powers of 800 kW, 12(d), 900 kW and 1 MW, a PIV signal loss is observed at the top right of the image. This can be linked to strong exchanges with the outside, particularly because of the high entrance of fresh air. This air supply leads to strong mixing resulting in a dilution of particles, hence less signal for PIV calculation. In addition, the velocity of hot gases increases

for powers from 100 kW to 500 kW but then appears to decrease. To confirm this hypothesis, Figure 14 is plotted.

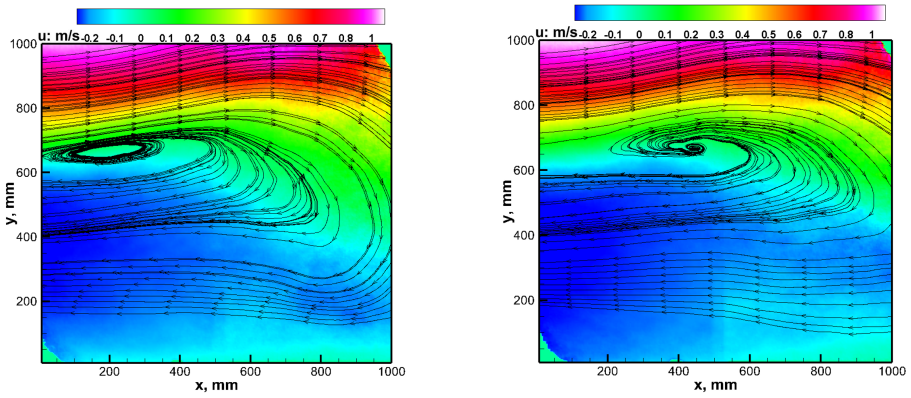

(a) (b)

FIGURE 13: Average velocity fields at 900 kW (a), 1000 kW (b).

The latter represents the evolution of the maximum average velocity present in the volume as a function of the input power. In this figure, a strong increase in the maximum velocity is observed for HRR from 100 kW to 500 kW. For the 600 kW case, the maximum velocity drops sharply, before rising slightly again for increased powers.

Under-ventilated conditions might explain the lack of oxidizer which limits the development of the fire and thereby the smoke dynamics. Indeed, for the power of 500 kW, 10 g/s of propane are fueling the burner. Considering that the combustion occurs at stoichiometric conditions i.e. for an adiabatic flame temperature of 2267K, there is around 1 m^3/s of hot gases which is produced. Considering a negligible pressure rise in the enclosure fire and the outlet area of 0.8 m^2 (clear aperture), the balance equations impose exit velocities of 1.25 m/s. This calculation resulting from first principals is in total agreement with the data of Figure 14, where the inflection point is between 1.42 and 1.12 m/s. Therefore, the analysis of Figure 14 shows that the velocity drop against power is clearly related to pressure rise in the chamber. Pressure rise induces accumulation of hot gases in the enclosure, which limits the volume of inlet fresh gases, hence under-ventilated conditions are reached.

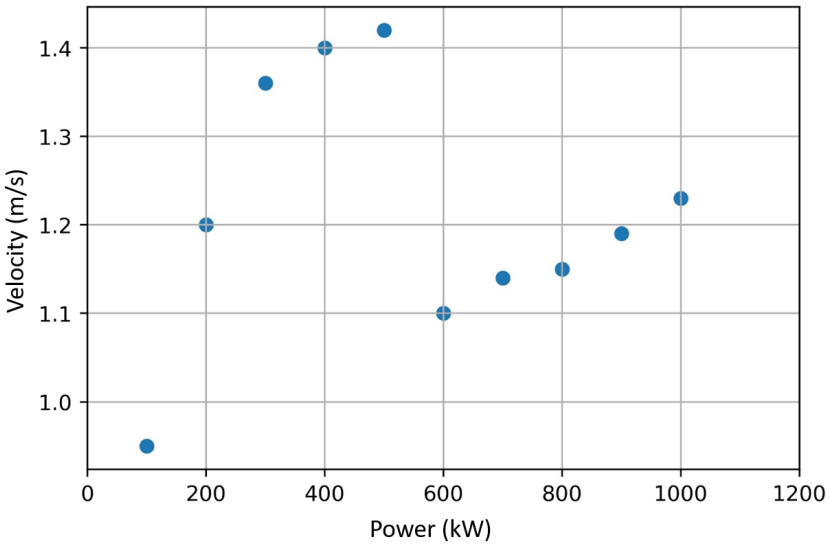

FIGURE 14: Exit velocity evolution as a function of power.

As a conclusion of the section, we demonstrated that from temperature profiles, HRR analysis and maximum velocity distribution seem to reveal conditions of well-ventilated and under-ventilated fires.

4.2.2. Comparison of numerical and experimental fields

To complete the analysis of the velocity fields, the results obtained numerically and experimentally are compared. In order to study cases in well-ventilated, poorly-ventilated and under-ventilated conditions, the HRR of 200 kW, 500 kW and 800 kW are considered. As a reminder, the studied configuration is available in the Figure 10. For each image presented below, the numerical field is located on the left while the experimentally measured field is on the right. Figure 15 shows the velocity fields for a power of 200 kW. On these two images, one can see that the numerical data overestimates the velocity in the upper part of the image. Moreover, the layer of hot fumes is more significant in the numerical image.
However, the velocities remain on the same order of magnitude. Although overestimated, the overall behaviour seems consistent with the experimental results. Figure 16 shows results for 500 kW.

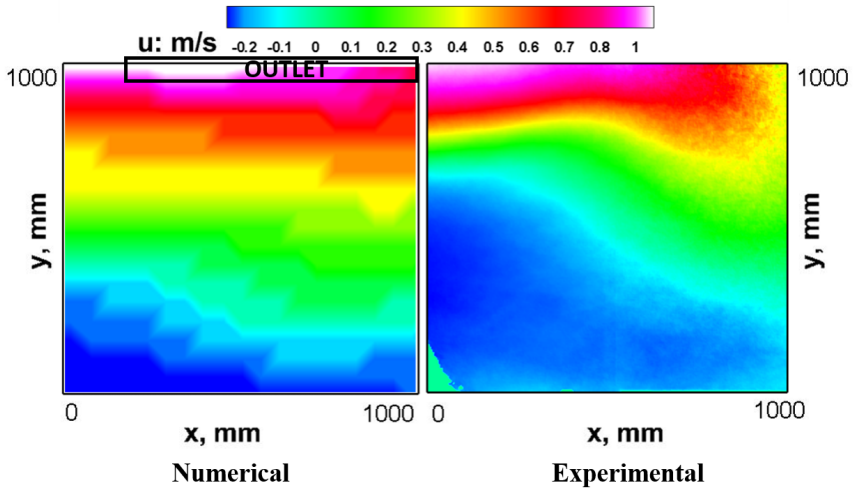

FIGURE 15: Comparison of numerical and experimental velocities, 200 kW.

The overall gas distribution is quite well simulated on the upper part of the image. The re-circulation of fresh gas towards the burner is slightly underestimated but maintains a coherent aspect with that observed experimentally by PIV.

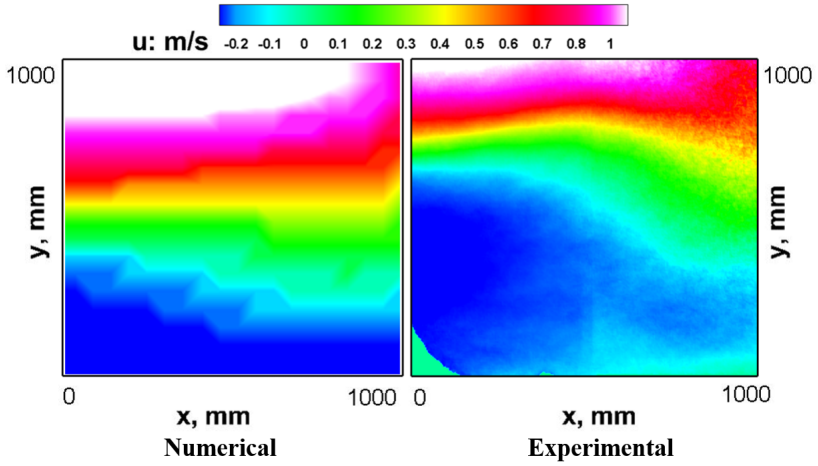

FIGURE 16: Comparison of numerical and experimental velocities, 500 kW.

To complete the analysis of the numerical and experimental velocities, the results obtained for a power of 800 kW are presented in Figure 17.
On the upper part of these images, a similarity in the velocity distribution and in the hot gas distribution can be observed.

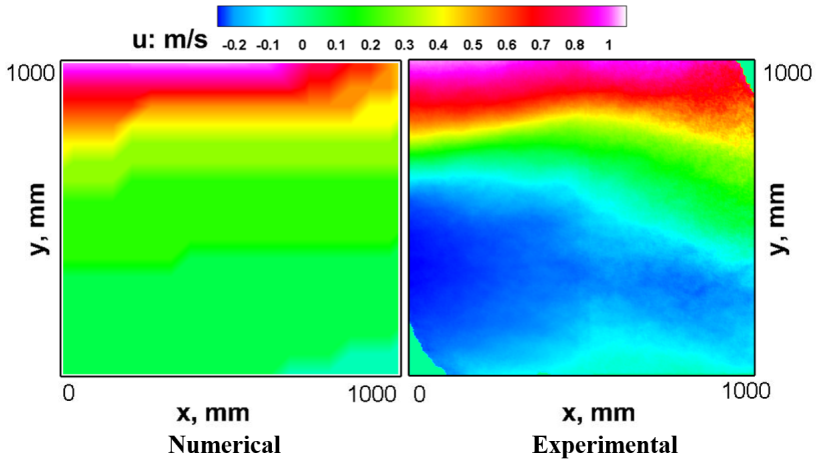

FIGURE 17: Comparison of numerical and experimental velocities, 800 kW.

However, the second part of the numerical image deviates from what is observed experimentally. Indeed, no fresh air return is present in the numerical results. One can incriminate the validity of the model in under-ventilated conditions.

4.2.3. Vertical velocities - Experimental measurements

Figure 18 shows the vertical component of the velocity profiles for 200 kW, 500 kW and 800 kW power ratings from experiments. In order to get as close as possible to the outlet, the velocities are measured in the upper part of the laser sheet. Velocities are plotted along the x axis.

The colours red, blue and black represent the HRR of 200 kW, 500 kW and 800 kW, respectively.

For the three cases, the first part of the figure (0 to 500 mm) indicates positive

velocities and therefore a hot smoke outlet. Higher HRR corresponded to higher velocities. This can linked to the increase of hot fumes which are released with increased powers.

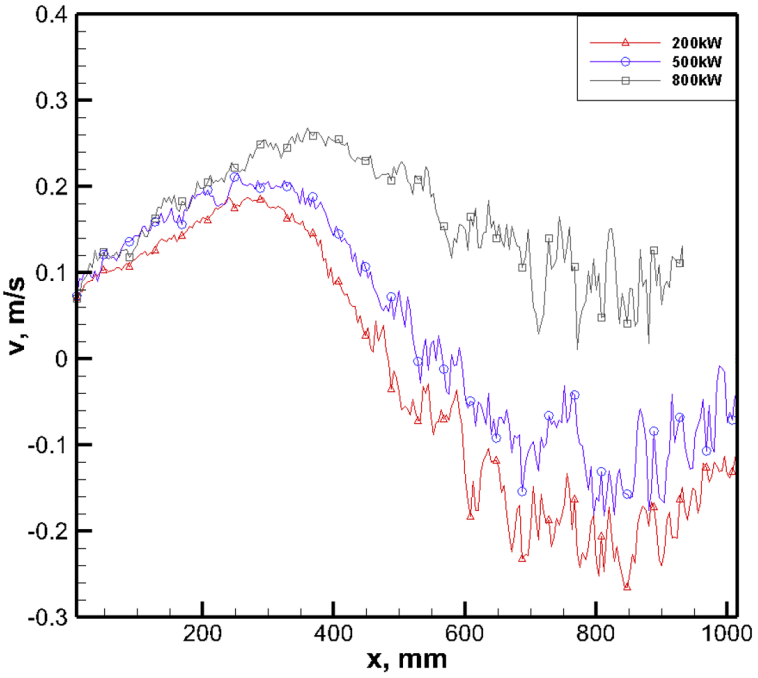

FIGURE 18: Comparison of vertical velocities

In the second part of the image, negative velocities are observed and therefore a fresh air return for 200 kW and 500 kW HRR exists. For the 800 kW power, no fresh air return is observed. Following this observation, oit can be concluded that hot fumes leaving the volume interfere with the entry of fresh air, resulting in only positive velocities.

5. Conclusion

In this study, the flow topology of a large scale confined fire is evaluated. The test cell is representative of a standard room and the power of the burner

went up to 1 MW. A dual approach is proposed. Experimental data for the scalar quantity temperature and 2D velocity fields are recorded and analyzed. Simulations using FDS are performed. The results are listed below.
First, the analysis of temperature evolution against time shows very good agreement between experimental data and simulation results since well - ventilated conditions are respected. For under-ventilated conditions, i.e. power of 800kW, discrepancies exist between the experimental and simulation results. FDS is shown to be inadequate for predicting under-ventilated conditions.
Second, large scale PIV data are recorded below the outlet. Beyond the inherent difficulty in managing large scale PIV in confined environment, the position of the smoke layer is shown to be in sensitive to the power inside the test cell. However, an extension of the interface between hot gases and fresh gases is noticed.
Third, the comparison of PIV data with 2D fields extracted from the simulations showed that good agreement exists for well-ventilated conditions.
Fourth, the evaluation of the maximum velocity against power revealed the clear existence of two behaviors. One for powers below 500 kW, where the maximum velocity is growing with the HRR and one for powers above 500 kW where a strong drop in the maximum velocity is observed before growing again. This illustrates the existence of a quantity which qualifies the ventilated status of the cell.
Fifth, the velocity profiles of the vertical component along the x-axis are evaluated for both well-ventilated and under-ventilated conditions. For ventilated conditions, it is shown that a well-established structure where fresh air and hot fumes enter and exit the cell exists. However, for under-ventilated conditions there is no significant fresh air inlet and only the air provided by the injection system facilitates combustion.
In conclusion, the clear existence of well-ventilated and under-ventilated conditions from temperatures and velocity fields is demonstrated. The experimental data is in agreement with the numerical data under well-ventilated conditions. Moreover, we pointed out the criteria based on flow dynamics that might make it easier the determination of ventilation status considering large scale confined fires.

6. Acknowledgements

Financial support from the French National Research Agency, under the project 'Firediag' is gratefully acknowledged. This project has been funded with the support from the European Union with the European Regional Development Fund (ERDF) and from the Regional Council of Normandie. The authors thank the computing center CRIANN for the computation time.

References

[1] B. Betting, Etudes Expérimentales et lois prédictives des foyers d'incendies, Ph.D. thesis, Normandie Université, 2018.

[2] B. Betting, É. Varea, C. Gobin, G. Godard, B. Lecordier, B. Patte-Rouland, Experimental and numerical investigations of the flow characteristics in confined fires, in : Journal of Physics : Conference Series, volume 1107, 2018.

[3] D. T. Gottuk, M. J. Peatross, J. P. Farley, F. W. Williams, The development and mitigation of backdraft : a real-scale shipboard study, Fire Safety Journal 33 (1999) 261 – 282.

[4] P. Bepoix, Les phénomènes thermiques, Editions Carlos Zaglia, 2015.

[5] J. Francis, A. Chen, Observable characteristics of flashover, Fire Safety Journal 51 (2012) 42 – 52.

[6] P. Thomas, M. Bullen, J. Quintiere, B. McCaffrey, Flashover and instabilities in fire behavior, Combustion and Flame 38 (1980) 159 – 171.

[7] S. Bishop, P. Holborn, A. Beard, D. Drysdale, Nonlinear dynamics of flashover in compartment fires, Fire Safety Journal 21 (1993) 11 – 45.

[8] N. Johansson, S. Svensson, Review of the use of fire dynamics theory in fire service activities, Fire Technology 55 (2019) 81–103.

[9] B. Merci, T. Beji, Fluid mechanics aspects of fire and smoke dynamics in enclosures, CRC Press, 2016.

[10] L. Bengtsson, Enclosure fire, Swedish Rescue Services Agency, Karlstad, Sweden, 2001.

[11] H. Prétrel, W. L. Saux, L. Audouin, Pressure variations induced by a pool fire in a well-confined and force-ventilated compartment, Fire Safety Journal 52 (2012) 11 – 24.

[12] B. McCaffrey, G. Heskestad, A robust bidirectional low-velocity probe for flame and fire application, Combustion and Flame 26 (1976) 125 – 127.

[13] S. Tieszen, T. O'Hern, R. Schefer, E. Weckman, T. Blanchat, Experimental study of the flow field in and around a one meter diameter methane fire, Combustion and Flame 129 (2002) 378 – 391.

[14] X. C. Hou, J. P. Gore, H. R. Baum, Measurements and prediction of air entrainment rates of pool fires, volume 26, 1996, pp. 1453 – 1459.

[15] A. Koched, H. Pretrel, L. Audouin, O. Vauquelin, F. Candelier, Application de la piv sur un écoulement de fumée à un passage de porte induit par une source incendie, 13ième Congrès de Techniques Laser, CFTL 2012 (2012).

[16] R. A. Bryant, A comparison of gas velocity measurements in a full-scale enclosure fire, Fire Safety Journal 44 (2009) 793 – 800.

[17] R. A. Bryant, G. W. Mulholland, A guide to characterizing heat release rate measurement uncertainty for full-scale fire tests, Fire and Materials 32 (2008) 121–139.

[18] A. Koched, H. Prétrel, O. Vauquelin, L. Audouin, Utilisation de la stereo piv pour l'optimisation des mesures de vitesse de fumee d'incendie a un passage de porte par des sondes bidirectionnelles, 14eme Congrés Francophone de Techniques Laser (CFTL2014) Marseille (2014).

[19] S. Desanghere, Détermination des conditions d'échauffement de structure extérieure à un bâtiment en situation d'incendie, Ph.D. thesis, INSA de Rouen, 2006.

[20] K. Mcgrattan, B. Klein, S. Hostikka, J. Floyd, Fire dynamics simulator user's guide, NIST special publication 1019 (2007) 5th Edition.

[21] K. Mcgrattan, S. Hostikka, J. Floyd, H. Baum, R. Rehm, Fire dynamics simulator (version 5) technical reference guide, NIST Special Publication 1018 (2007) 5th Edition.

[22] B. A. Magnognou Sambouni, Etudes numériques et expérimentales sur le risque d'inflammation des gaz imbrûlés au cours d'un incendie en milieu sous-ventilé, Ph.D. thesis, 2016. Ecole Nationale Supérieure de Mécanique et d'Aérotechnique.